Hindawi
Mathematical Problems in Engineering
Volume 2020, Article ID 8084941, 14 pages
https://doi.org/10.1155/2020/8084941

Research Article

Research on the Optimization Design of Abnormal Flip Buckets

Liang-ze-nan Wang and Chao Su

College of Water Conservancy and Hydropower Engineering, Hohai University, Nanjing 210098, China

Correspondence should be addressed to Liang-ze-nan Wang; 1245505414@qq.com

Received 8 January 2020; Revised 25 March 2020; Accepted 30 March 2020; Published 23 April 2020

Academic Editor: Giorgio Besagni

This study constructs an optimization model to address ski-jump energy dissipation problems in different reservoir environments. The multiobjective genetic algorithm is herein applied as the calculation method. In the process of changing the ski-jump flow model, the runoff of ski-jump flow is changed (especially the abnormal flip bucket). Water flow might go from having a single falling point to multiple falling points. Optimization is only performed after the stabilization of the fall of the water because the fall of the water from the starting point to the ground is not stable over a short period. Only a stable flow can reduce the computation time for optimization. The optimal overflow width and height of the flip bucket were calculated through optimal computation, which can minimize the scouring force of the water flow as it falls to the ground. The results obtained provide theoretical references for practical engineering and reduce the potential safety hazards. The energy in flip buckets following the optimization of the water flow can be fully dissipated, creating an ecosystem where water can flow unobstructed. Guiding a water flow to water-deficient areas is of great significance in ensuring the long-term protection of environments and ecosystems.

1. Introduction

Ski-jump energy dissipation is the common energy dissipation mode in water bodies and in hydropower engineering. With its simple structural design and its economical and practical performance, ski-jump energy dissipation is often the first choice in practical engineering situations [1]. There are many influential factors during the process of ski-jump energy dissipation. This study focuses not only on full ski-jump energy dissipation but also on the scouring effect as water flows to the ground. Therefore, achieving an optimal design in a ski-jump flow requires the consideration of two factors: (1) the interaction of streams, such as the maximum dissipation and adulteration of high-speed water flow in the air and (2) controlling the shape and scouring force of a water flow as it flows to the ground in order to realize the minimum scouring force and range [2, 3].

In middle- and high-release structures, flow kinetic energy is high and it is often used in ski-jump energy dissipation. Water flows out of the flip bucket and decelerates in the air due to resistance, accompanied by a reduction in kinetic energy. Water flows to the ground and forms scouring pits. With an increase in scouring time, fixed scouring pits are formed and kinetic energy again decreases, thus resulting in the effect of energy elimination. Given the allowable environmental and topographical conditions in downstream regions, ski-jump energy dissipation is often an appropriate choice, but consideration must be given to atomized rain [4].

The shapes of the bottom and side walls in abnormal flip buckets are diverse. There are various combinations that take many practical conditions into consideration. In terrain environments, the falling point of a water flow often has to be controlled at a preset position to protect the terrain. This can be realized by changing the shape of the flip bucket so as to change the direction of the water flow [5, 6].

The ski-jump spillway is a compact structure designed to release the dam overflow. In this dissipation system, the flow digs a scour hole in the river bed, which is shape dependent on the rock bed resistance as well as the effort caused by the jet. Numerical modeling of the hydraulic phenomenon through computational fluid dynamic (CFD) approaches is one of the main parts of high-cost hydraulic structure studies [7]. To model hydraulic characteristics, several methods such as physical and numerical methods can be used. Nowadays, by utilizing new methods in computational fluid dynamics

(CFD) and with the development of fast computers, numerical methods have become accessible for use in the analysis of such sophisticated flows [8, 9]. Studies on the flow through the hydraulic structures are usually conducted using physical modeling. Physical modeling is based on basic fluid mechanic equations. The physical modeling of hydraulic structures means that a scaled laboratory model of the prototype is constructed; this approach is a safe way to analyze the flow through or over the hydraulic structures. Due to the high cost of laboratory experiments, researchers have attempted to use numerical simulations along with physical modeling [10–12]. Flow pattern recognition that uses physical modeling and numerical simulations helps designers to propose an optimal shape for hydraulic structures. The optimal shape of a hydraulic structure can result in an increase in their performance [13].

In this paper, the influence of the overflow width and height of the flip bucket on the pressure of the water falling point, as well as the kinetic energy at the falling point, have been studied. When the overflow width and height of the flip bucket are fixed, the optimization is then geared toward attaining minimum absolute values for pressure and kinetic energy at the falling point of water flow by using a genetic algorithm. The final optimization goal is to study the influence of the model design size of the abnormal flip bucket on ski-jump flow and to provide theoretical guidance for experimental simulations and practical engineering. Our results demonstrate that pressure intensity and kinetic energy were reduced compared with the original program, indicating that reasonable optimization results had been obtained.

1.1. Experimental Section

1.1.1. Right Triangular Thin-Walled Weir Flow. The right triangular thin-walled weir flow was applied by adjusting the water gate to change the flow rate. The flow rate could not be read directly but had to be calculated using the formula $Q = C_0 H^{2.5}$ after the head on the weirs (H) was read through the U-shaped connector. In the formula, C_0 is the flow coefficient of the right triangular thin-walled weir flow, which is generally $C_0 = 1.4$.

When $H > 25$cm, the calculation formula is revised as $Q = 1.343H^{2.47}$, where Q is the flow rate (m^3/s) and H is the head of the weirs (m) [14].

1.1.2. Rectangular Thin-Walled Weir Flow. The flow rate of a nonsubmerged rectangular thin-walled weir without lateral shrinkage was calculated as $Q = mb\sqrt{2g}H_0^{1.5}$. The flow rate was adjusted continuously for multiple measurements. The stage-discharge curve was drawn based on the measured results. Finally, the flow coefficient (m) was calculated [15].

1.1.3. Indexes for Cavitation Judgment: the Number of Cavitations. The one-dimensional number of cavitations is often used as the measurement index of cavitations in actual water flow when studying cavitation problems, which is expressed as K:

$$K = \frac{p - p_v}{(1/2)\rho v^2} = \frac{(p - p_v)/\rho g}{(v^2/2g)}, \quad (1)$$

where p and v are the absolute pressure intensity and the average flow rate at the places where the water flow was not influenced by the local variation of boundaries, p_v is the steam pressure, and ρ is the water density.

The primary number of cavitations is determined by the boundary conditions. For some boundary profiles, the number of cavitations is a fixed number and is often determined by the experiment.

The number of cavitations in an actual water flow (K) and the primary number of cavitations (K_i) were compared. When $K > K_i$, no cavitation was formed. When $K \le K_i$, there was a cavitation [16].

1.2. Experimental Project. The total capacity of the studied reservoir was 49.921 million m^3, and the normal pool level was 2048.50 m. The design flood level ($P = 2\%$) was 2047.90 m (major flood period), and the discharged volume of the spillway tunnel was 88.90 m^3/s. The maximum flood level ($P = 0.1\%$) was 2050.85 m, and the discharged volume of the spillway tunnel was 135.00 m^3/s. The flood standard for the downstream energy dissipation and erosion control was a frequency of 30 years ($P = 3.33\%$), and the discharged volume of the spillway tunnel was 88.50 m^3/s.

The spillway tunnel was reconstructed from a diversion tunnel (Figure 1). It is on the right dam abutment and covers a length of 450.60 m (horizontal distance), including the inlet section, the repairing chamber section, the Longtaitou section, the pressure section, the working chamber section, and the outlet energy dissipation section. The floor elevation of the inlet horn section ($0 + 000.000 \sim 0 + 003.200$) was 2007.00 m, which is connected to a 48.80 m long round pressure section with a hole diameter of 3.20 m. The repairing chamber section was ($0 + 062.000 \sim 0 + 068.000$) 6.00 m long. A 10.00 m long round-to-square pressure slope section (D3.2 m $\longrightarrow$ 2.8×2.8 m) was set on the upstream side and another 10.00-m-long square-to-round section (3.2×3.2 m $\longrightarrow$ D3.2 m) was set on the downstream side. The Longtaitou section was $0 + 078.000 \sim 0 + 129.447$, with a hole diameter of 3.20 m. The round pressure section was $0 + 129.447 \sim 0 + 410.600$, where the hole diameter was 3.20 m, and the longitudinal slope was 1/200. The working chamber section ($0 + 416.000 \sim 0 + 430.600$) was 14.00 m long, and a 6.00 m long round-to-square pressure slope section (D3.2 m $\longrightarrow$ 2.5×2.5 m) was set up on the upstream. Subsequently, the outlet section of the ski-jump energy dissipation (Figure 2) was established, which was 20.00 m long and 2.50 m wide. The elevation at the top of the flip bucket was 1980.724 m, the arc radius was 20.00 m, and the ski-jump angle was 25°. An area downstream from the flip bucket was connected to a 10.00 m long apron.

1.3. Flip Bucket of the Spillway Tunnel. The coverage and the horizontal length of the arc section of the spillway tunnel were kept constant while the arc radius decreased from 20.00 m to 10.00 m. The ski-jump angle was gradually

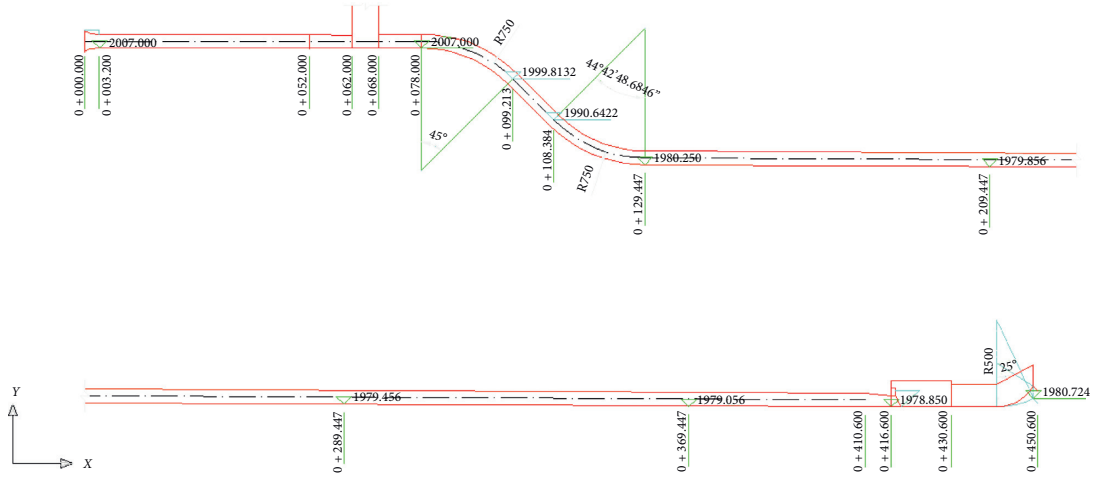

Figure 1: Positions of sections in the model.

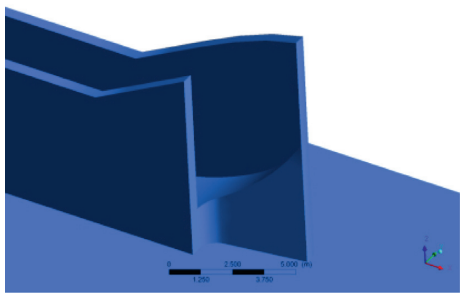

Figure 2: Three-dimensional diagram of the outlet section of the spillway tunnel.

changed from 57°41′50.2306″ to 25° from the left to the right. The elevation of the nose of the weir at the left wall was 1983.506 m, and the elevation on the right wall was 1979.787 m. The right wall of 0 + 441.148 ~ 0 + 449.600 was eliminated, while the left wall deflected toward the downstream from 0 + 444.267 at a radius of 12 m on the plane. An oblique nose of the weir was set from the ski-jump angle of 0° at the right wall to the axis of the 0 + 449.600 mileage. Meanwhile, the ski-jump flow was measured close to the nose weir to prevent too great an angle in the right flow. An arc connected to the oblique nose weir with a plane radius of 0.724 m was set in position (0 + 445.374) with a ski-jump angle of 25° on the right wall. The design of the abnormal flip bucket is shown in Figure 3.

1.4. Experiment of the Spillway Tunnel

1.4.1. Experimental Design. The model was designed according to gravity similarity, and a normal model was applied. According to the calculations and comparisons, the final scale of the model was λL = 40, and the corresponding scale parameters were as follows:

Flow scale: λQ = λL ∗ 5/2 = 10119

Time scale: λT = λL/2 = 6.325

Flow rate scale: λV = λL/2 = 6.325

Roughness scale: λn = λL/6 = 1.849

1.4.2. Experimental Manufacturing. The downstream terrain at the outlet of the spillway tunnel started from the arc section. It was mainly filled with scouring materials and cement dies. The pressure section and nonpressure section of the spillway tunnel were manufactured using organic glass according to the shape and size provided by the design unit (Figure 4). The roughness rate met the experimental requirements (the roughness rate of organic glass was $n = 0.007 \sim 0.009$, the roughness rate of concrete was $n = 0.014 \sim 0.017$, and the roughness scale of the prototype and model was 1.56 ~ 2.43).

1.5. Water Jet Shape of the Spillway Tunnel and Downstream Scouring. Taking into consideration the energy dissipation and erosion control during a flood, which occurs once every 30 years ($P = 3.33\%$), the water depth on the left increased to 2.40 m as the water flow at the outlet section was influenced by wall deflection, while on the right, the depth of the water did not significantly change. The cross section of the outflow was approximately a Z-shaped section. The jet trajectory length of the left flow was 72 m, and the water flow fell by 18 m on the right of the axis (downstream). The greatest height of the middle water jet was 24 m, and the jet trajectory length was 96 m, while the water flow fell by 30 m to the right of the axis (downstream). The right-hand water flow was injected by different layers (the upper water flow was injected along the axis and the lower water flow was injected along the axis toward the right at 25°). The jet trajectory length was 30 m. The lower edge of the water jet was only 2.40 m away from the water surface (depth of water = 3.2 m). After continuous scouring over a period of 4 h, the left-hand flow and the middle flow dropped, without a scouring pit formation. The scouring pit of the right-hand flow was 5.50 m long, 5.00 m wide, and 2.40 m deep.

Taking into consideration energy dissipation and erosion control during flood conditions, the water jet from the spillway tunnel is shown in Figure 5, which is approximately "Z-shaped". The water jet from the bottom layer is shown in Figure 6.

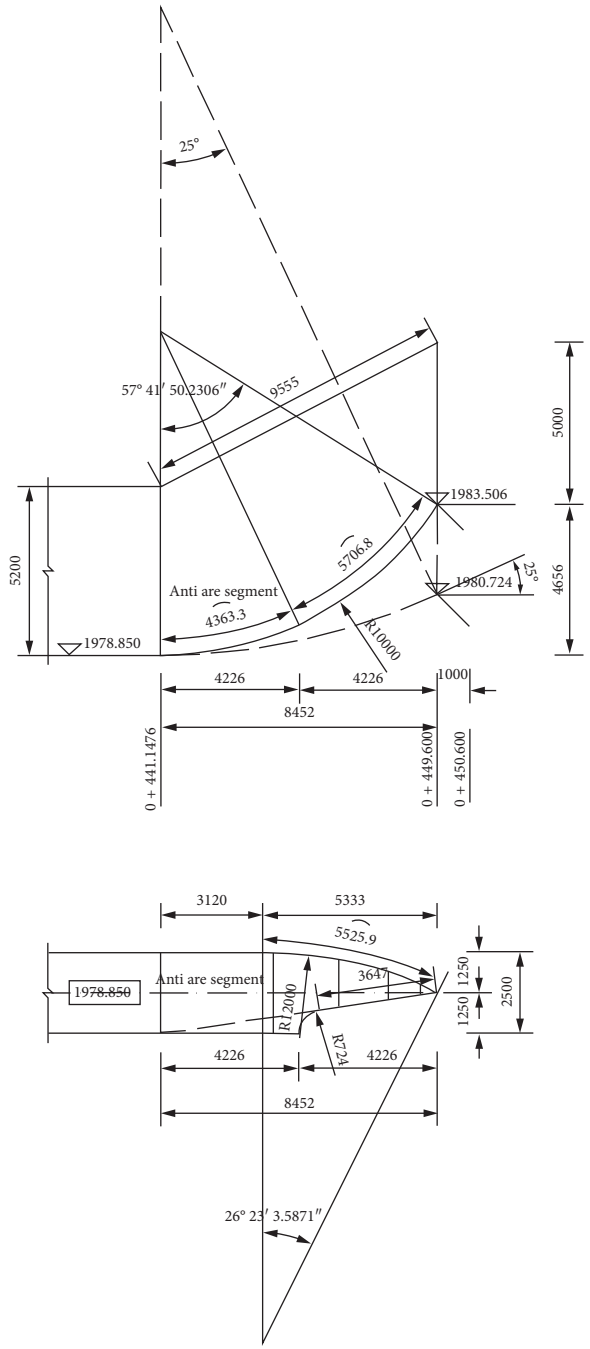

Figure 3: Design of the abnormal flip bucket.

2. Numerical Simulation in Contrast with the Experimental Results of the Abnormal Flip Bucket

2.1. Standard $k-\varepsilon$ Model. The standard $k-\varepsilon$ model requires the turbulence energy and the dissipation rate equation to be solved. The transport equation of the turbulence energy is deduced from an accurate equation, while the dissipation rate equation is inferred from physics and is gained from the mathematical simulation of similar round equations. The standard $k-\varepsilon$ model hypothesizes that the flow has full turbulence, and the influences of molecular viscosity can be neglected. Therefore, the standard $k-\varepsilon$ model is only applicable to simulations of the complete turbulence flow process. This model was proposed by Spalding and Launder in 1972 [16, 17]. The dissipation rate of turbulence (ε) is defined as follows:

$$\varepsilon = \frac{\mu}{\rho}\overline{\left(\frac{\partial u_i'}{\partial x_k}\right)}. \tag{2}$$

The turbulence viscosity coefficient is μ, which can be expressed as the function of k and ε:

$$\mu_t = \rho C_\mu \frac{k^2}{\varepsilon}. \tag{3}$$

Figure 4: Experimental model of the ski-jump flow section in the spillway tunnel.

Figure 5: Left view of the ski-jump flow experiment in the spillway tunnel.

Figure 6: Right view of the ski-jump flow experiment in the spillway tunnel.

In the standard $k-\varepsilon$ model, the transport equation of k and ε is introduced as follows.

The k equation is

$$\frac{\partial(\rho k)}{\partial t}+\frac{\partial(\rho k u_i)}{\partial x_i}=\frac{\partial}{\partial x_j}\left[\left(\mu+\frac{\mu_i}{\sigma_k}\right)\frac{\partial k}{\partial x_j}\right] + G_k + G_b - \rho\varepsilon - Y_M + S_k. \tag{4}$$

The ε equation is:

$$\frac{\partial(\rho\varepsilon)}{\partial t}+\frac{\partial(\rho\varepsilon u_i)}{\partial x_i}=\frac{\partial}{\partial x_j}\left[\left(\mu+\frac{\mu_i}{\sigma_\varepsilon}\right)\frac{\partial\varepsilon}{\partial x_j}\right]+C_{1\varepsilon}\frac{\varepsilon}{k}\left(G_k+C_{3\varepsilon}G_b\right) - C_{2\varepsilon}\rho\frac{\varepsilon^2}{k}+S_\varepsilon, \tag{5}$$

where G_b is the production term caused by buoyancy. For incompressible fluid, $G_b = 0$. For compressible fluid,

$$G_b=\beta g_i\frac{\mu_i}{\mathrm{Pr}_i}\frac{\partial T}{\partial x_i}, \tag{6}$$

where Pr_i is the turbulent Prandtl number, $\mathrm{Pr}_i = 0.85$ in this model, g_i is the gravitational acceleration, and β is the coefficient of thermal expansion:

$$\beta=-\frac{1}{\rho}\frac{\partial\rho}{\partial T}. \tag{7}$$

G_k is the production term of the turbulence energy (k), and it is caused by the average velocity gradient:

$$G_k=\mu_i\left(\frac{\partial u_i}{\partial x_j}+\frac{\partial u_j}{\partial x_i}\right)\frac{\partial u_i}{\partial x_j}. \tag{8}$$

For incompressible fluid, $Y_M = 0$. For compressible fluid,

$$Y_M=2\rho a M_t^2, \tag{9}$$

where a is the sound velocity and $a=\sqrt{\gamma RT}$ and M_t is the turbulence Mach number and $M_t=\sqrt{k/a^2}$.

In the standard $k-\varepsilon$ model, $C_\mu = 0.09$, $\sigma_\varepsilon = 1.3$, $C_{1\varepsilon} = 1.44$, and $\sigma_k = 1.0$.

The standard $k-\varepsilon$ model is the simplest complete two-equation turbulence model, which has wide applicability, is economical, and achieves reasonable accuracy. It is extensively applied in the industrial flow field and in heat-exchange simulations [18, 19].

2.2. Comparison of Calculated Results. The greatest height of the water jet and the jet trajectory length were calculated as 22.88 m and 91.64 m, respectively. The simulation results are shown in Figure 7, Figure 8, Figure 9, and Table 1.

2.3. Analysis of Calculated Results

2.3.1. Contrast Analysis of the Theoretical Values and Experimental Values. Three conclusions can be drawn from Table 1.

Conclusion 1: the theoretical value of speed is generally consistent with the actual value of the speed.

Conclusion 2: water flows in the pressure circular tube to keep a constant flow velocity.

Conclusion 3: the water flow rate increases suddenly after the gate and then decreases gradually. Using the calculated results, the software can effectively simulate the whole water flow process [20].

2.3.2. Analysis of the Relationship between the Theoretical Value and the Actual Environment. It can be seen from Figure 7 that the ski-jump flow only has one falling point in the numerical simulation. The greatest height of the water jet and the jet trajectory length are calculated as 22.88 m and 91.64 m, respectively. These two parameters are similar to those in the experiment (24 m and 96 m, respectively). To calculate the jet trajectory length, attention should be paid to the position with the deepest scouring pit. The actual jet trajectory length is different from the theoretical value. According to different engineering cases, the actual jet trajectory length greatly differs from the theoretical value due to variations in environmental conditions in real-world scenarios. These include thin air, low atmospheric pressure, and small resistance in plateau regions with high altitudes. However, there is high atmospheric pressure and strong resistance in plain regions with low altitudes. In windy regions, water flow experiences aerated flow dissipation due to the influence of winds. The calculation of such aerated flow dissipation is highly complicated, and it is difficult to express through mathematical equations [17, 21]. The pressure intensity distribution is shown in Figure 8, and the volume rendering of the volume fraction of the water flow is shown in Figure 9.

3. Multiobjective Optimization Design of the Abnormal Flip Bucket

The complicated optimization of a ski-jump flow involves many problems. In the process of changing the ski-jump flow model, the runoff of the ski-jump flow is changed (especially the abnormal flip bucket). Water flow might go from having a single falling point to multiple falling points. In the optimization of a high-speed water flow, optimization goals were set to obtain maximum kinetic energy and pressure at all water falling points. Therefore, the minimums among these maximums would provide the optimal scheme [22].

3.1. Multiobjective Optimization Model

3.1.1. Objective Function. Due to the influence of ski-jump energy dissipation on the scouring pit in real-life engineering situations, the pressure of the water flow at the falling point influences the depth of the scouring pit, while the kinetic energy of the water flow influences its shape. The optimization objective is determined at the minimum water flow pressure at the falling point, where the minimum

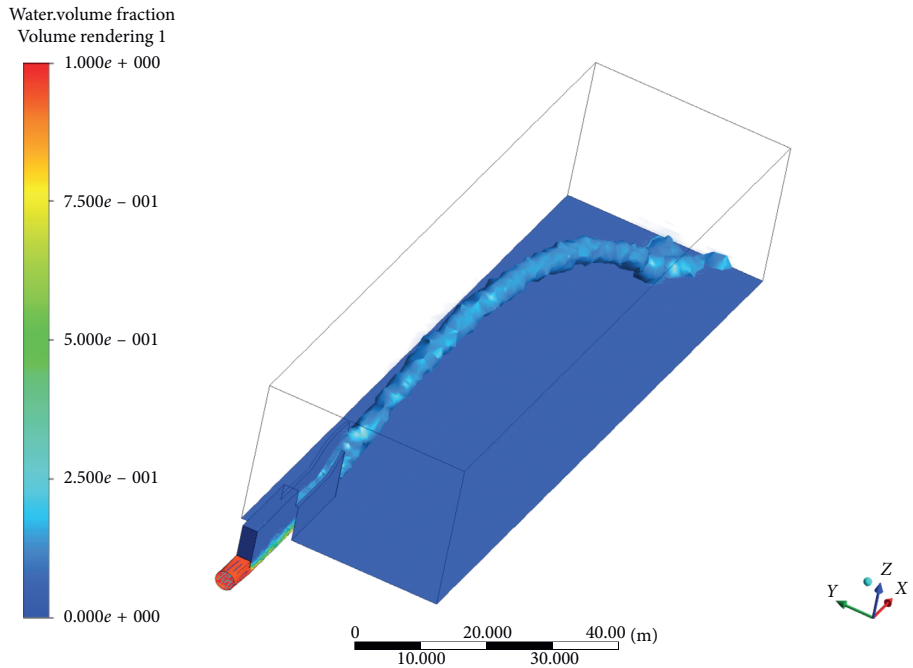

Figure 7: Numerical simulation of the abnormal flip bucket.

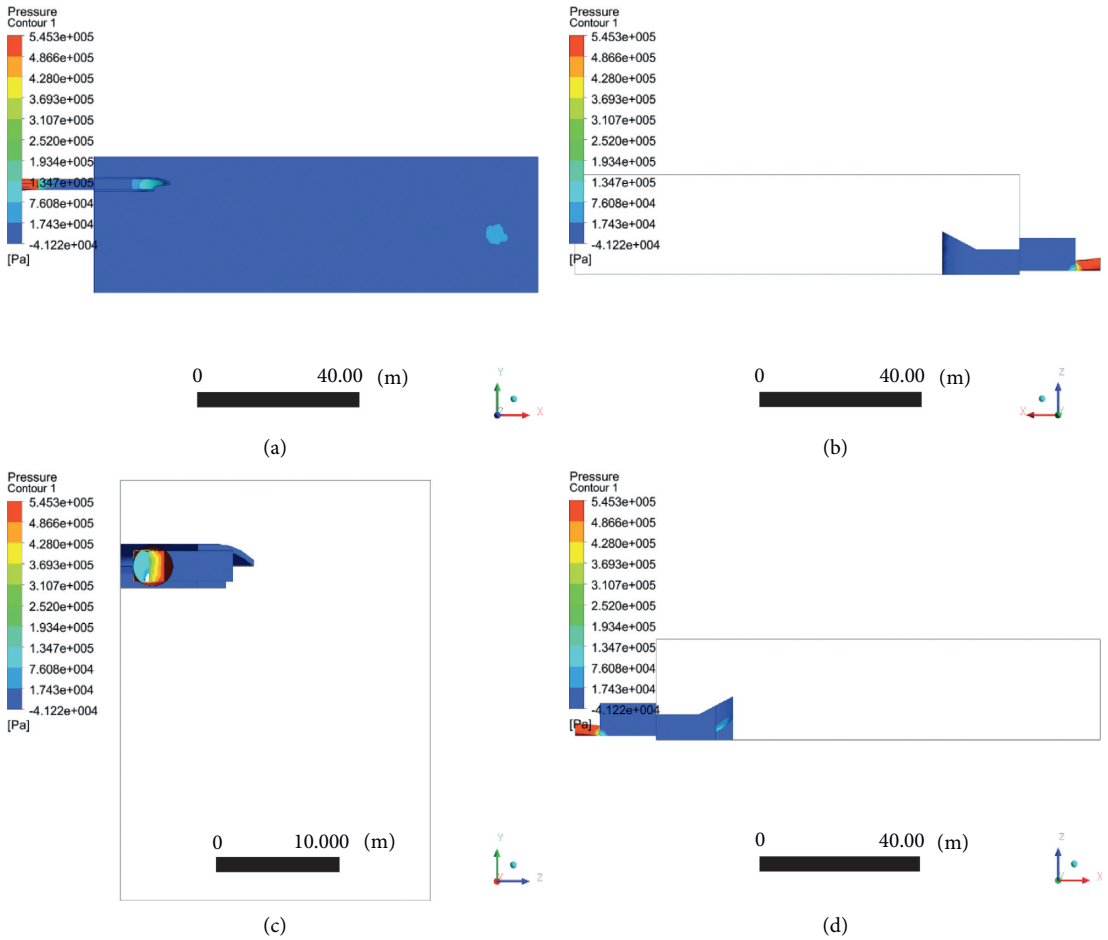

Figure 8: Pressure contour.

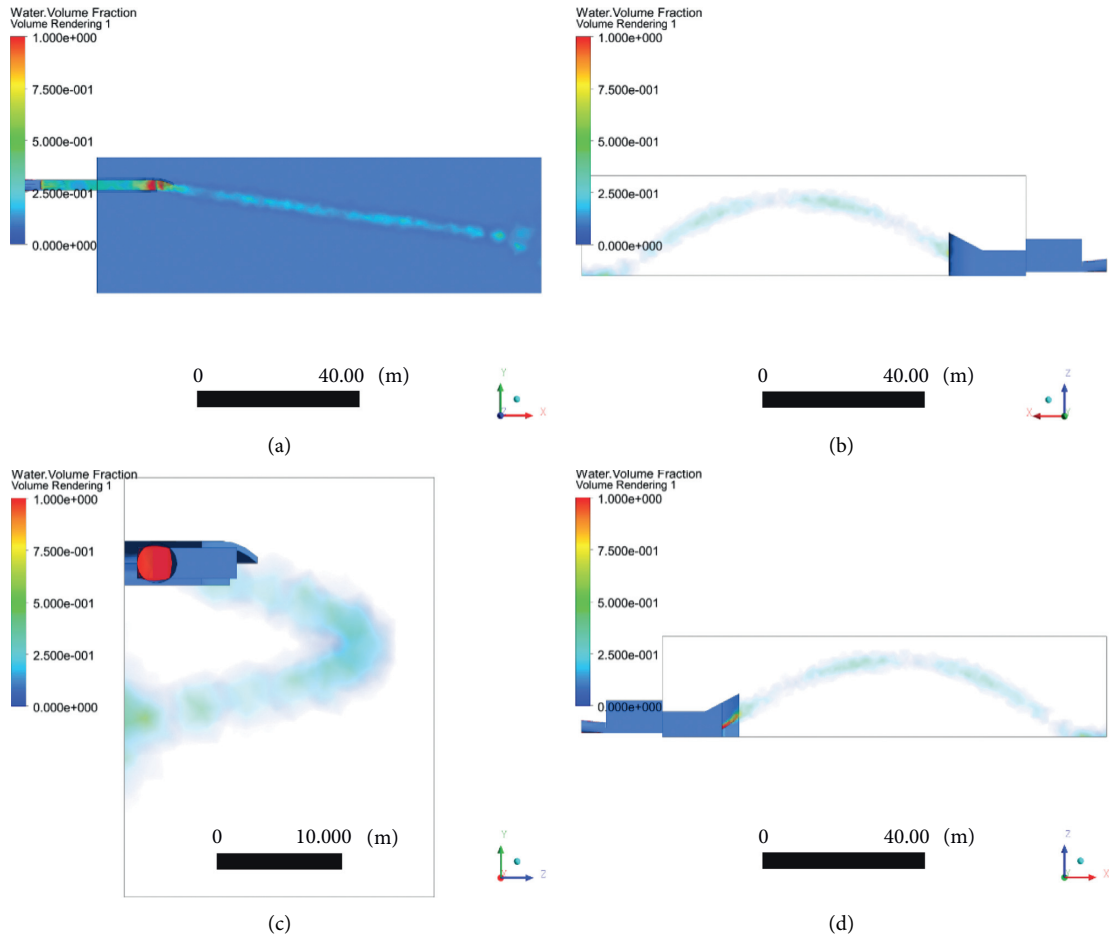

Figure 9: Volume rendering.

Table 1: Hydraulic elements of the spillway tunnel $Q = 71.96\ m^3/s$ (P = 3.33%).

Number of measuring points	Mileage	Measured flow rate (m/s)	Calculated flow rate (m/s)	Notes
1	0 + 052.000	8.95	8.95	Round-to-square
2	0 + 062.000	9.18	9.06	
3	0 + 064.500	9.18	6.77	Maintenance
4	0 + 064.500	9.18	6.77	
5	0 + 068.000	7.03	7.81	Square-to-round
6	0 + 078.000	8.95	8.97	
7	0 + 105.000	8.95	8.92	Longtaitou
8	0 + 129.447	8.95	8.94	
9	0 + 410.200	8.95	9.01	
10	0 + 411.000	8.99	9.16	Pressure slope section
11	0 + 416.600	11.51	12.84	
12	0 + 420.600	31.82	32.46	After the gate
13	0 + 442.148	28.89	27.25	Arc section
14	0 + 450.600	27.77	24.79	

kinetic energy is measured. The objective function is the minimum pressure caused by the water flow impacting on walls and the minimum impact velocity of the water falling on the walls. Since the pressure is negative, its maximum is set as 0. The geometric model corresponding to the minimum pressure and minimum speed at the falling point has to be identified.

3.1.2. Design Variables. The overflow width of the flip bucket and the height of the water from the flip bucket (height of the flip bucket) were defined as the design variables. They are direct influencing factors on the width and the height of the water jet. The height of the flip bucket influences different arc angles in the modeling. Therefore, the angle was not used as a design variable [3, 23, 24].

3.1.3. Constraint. The boundary condition of the flip bucket model was used as one constraint for the optimization of ski-jump energy dissipation. The inlet flow rate was kept constant, and it was used as another constraint. The movement range of the ski-jump flow in the air was defined as a constraint, and a reasonable size range of the flip bucket was determined according to that in the experimental model, which was viewed as another constraint. The optimal solution could be found within this range [19, 25].

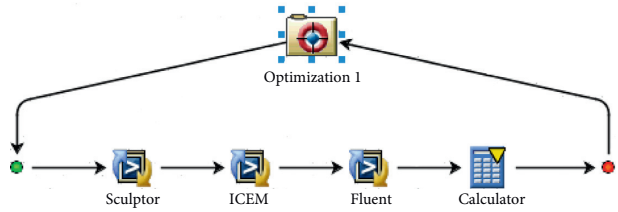

Figure 10: Calculation procedure for Isight software.

3.1.4. Optimization Algorithm. It is necessary to choose multiple objectives in the optimization of the flip bucket. The ski-jump flow process is highly complicated. Having a single objective makes it difficult to find a relatively reasonable optimization result [26]. The multiobjective optimization algorithm can generally be divided into two types: the normalized type and the nonnormalized type.

A normalized multiobjective optimization algorithm changes multiple objectives into a single objective for optimization, and the weight is determined subjectively by the optimizer rather than the decision maker. The normalized multiobjective optimization algorithm is very sensitive to the optimal leading shape of the Pareto distribution. It can neither process the leading valley of the Pareto distribution nor does it have high problem-solving efficiency.

The nonnormalized multiobjective optimization algorithm processes multiple objectives directly through the Pareto mechanism. It does not have to transform multiple objectives into a single objective to make the leading edge of the solving set as close as possible to the leading edge of Pareto. Meanwhile, the leading edge of Pareto can be covered uniformly. The nonnormalized multiobjective optimization algorithm is a multiobjective genetic algorithm. In this study, the multiobjective genetic algorithm NSGA-II was applied [27].

3.1.5. Optimal Design scheme 1. A model was constructed, and it was then meshed well. The model was input into the sculptor software, which was used for the deformation of the grids of the flip bucket. Later, the grids were processed using ICEM and calculated using the Ansys fluent software. Finally, the sculptor software ICEM and the Ansys fluent software of the model were integrated using Isight software (Figure 10).

Advantages include the fact that parameterization of the calculation model was not necessary. A model was constructed and then meshed, the grid deformation was carried out directly by the sculptor software of the design model, and the model size was changed. Grids were processed by ICEM, and the Ansys fluent software was applied for calculation. Finally, the optimal computation was performed after integration with the Isight software. Moreover, the optimal design scheme 1 has a high operation speed and saves time. Moreover, it does not construct a model for every computation.

Disadvantages include the simulation accuracy of the sculptor software in the model deformation being lower than that of parameterization modeling.

3.1.6. Optimal Design scheme 2. For parameterization of the model in the Ansys software, the mathematical relation among the initial design points had to be determined. Coordinates of 10 points in the initial design were calculated by solving the equation of a circle and a proportional method corresponding to the triangle similarity:

angle is the ski − jump angle,

r_1 is the ski − jump arc,

h_1 is height of the inlet wall,

h_2 is height of the outlet wall,

w is the inlet width,

r_2 is the radius of deflected arc,

r_3 is the radius of the arc, which is connected to the oblique flip bucket,

$$r_3 = \frac{wr_1 \sin(\text{angle})}{4\left(\sqrt{(r_1 \sin(\text{angle}))^2 + (w/2)^2} - (w/2)\right)},$$

$$
\begin{aligned}
&k_1\,(0,0,0),\\
&k_2\,(0,h_1,0),\\
&k_3\left(r_1\sin(\text{angle}),\frac{r_1}{2}+h_2-\sqrt{\frac{{r_1}^2}{4}-\left(r_1\sin(\text{angle})\right)^2},0\right),\\
&k_4\left(r_1\sin(\text{angle}),\frac{r_1}{2}-\sqrt{\frac{{r_1}^2}{4}-\left(r_1\sin(\text{angle})\right)^2},0,\right)\\
&k_5\,(0,0,1),\\
&k_6\,(0,0,1+w),\\
&k_7\left(r_1\sin(\text{angle})-\sqrt{{r_2}^2-\left(r_2-\frac{w}{2}\right)^2},0,1\right),\\
&k_8\left(\frac{r_1\sin(\text{angle})}{2},0,1+w\right),\\
&k_9\left(r_1\sin(\text{angle}),0,1+\frac{w}{2}\right),\\
&k_{10}\left(\frac{r_1\sin(\text{angle})}{2}+r_3\left(1-\frac{w}{2\sqrt{\left(r_1\sin(\text{angle})\right)^2+(w/2)^2}}+\left(\frac{w}{2}\right)^2\right),0,1+w-\frac{r_3r_1\sin(\text{angle})}{\sqrt{\left(r_1\sin(\text{angle})\right)^2+(w/2)^2}}\right).
\end{aligned}
\tag{10}
$$

The grid part cannot be directly realized in the workbench from the construction of the model to the gridding and, finally, to computation. Putting simply, this scheme requires the recording of the macroefficiency in the workbench to record the gridding program, which makes the scheme easier to use.

Advantages include this scheme being able to accurately determine the relationship between the model size and the optimization objective. Disadvantages, however, include each computation requiring the construction of a new model, followed by meshing. It often requires hundreds of repeated computations, or more, to realize the optimization objective. The model construction in each computation significantly increases the workload of the computer.

3.2. Reasons for Using Optimal Design scheme 1 as the Optimization Scheme. Optimal design 1 does not require modeling in each computation. Instead, it only has to draw the original design model, which changes according to the given size range. This requires a shorter computation time. Optimal design 2 requires the parameterization of the model, and a new model has to be constructed for each change to the computational model, thus resulting in a longer computation time. Therefore, the optimal design 1 was chosen for this study.

4. Results and Discussion

4.1. Optimization Results. The following optimization results were gained from repeated computations of different ski-jump flows based on the computer program:

4.2. Discussion of Optimization Results

4.2.1. Analysis of Computation Time. Based on the above results, the water pressure against the ground over different periods varies. Therefore, the optimal body cannot consider the optimal body simply at one time point. Moreover, attention should be paid to the corresponding period of the optimal body shape. By doing this, a reasonable optimal solution can be realized. In this study, this period is chosen to be 1 s. Hence, the optimal body shape can only be realized during this 1-s period, and only the optimal model during this 1 s is calculated. In Table 2, the optimal solution is to decrease the overflow width by 0.26574 m and decrease the height of the flip bucket by 0.23634 m. Compared with the original scheme, this optimal solution showed an 18.29% lower pressure intensity and 17.74% lower kinetic energy. To increase the accuracy of the research results, the computation time was increased by setting the time period as 10 s, for example. This can prolong the operation time of the computer. Optimization is only performed after the stabilization of the water fall because the water fall from the starting point to the ground is not stable over a short period. Only a stable flow can shorten the computation time for optimization [2, 25, 26].

4.2.2. Discussion of the Relationship between the Size of the Flip Buckets and the Hydraulic Elements. Relevant laws among hydraulic elements can be found from optimization. Optimization should consider not only the pressure of the falling points and the relationship between the flow velocity and the size of flip bucket [28] but also the relationship

Table 2: Comparison of the optimization results and the original design scheme.

Variables	Original design value	Optimal value
Pressure at falling points	−667pa	−545pa
Velocity arriving at the falling points	32.89 m/s	29.83 m/s
Overflow width	3.2 m	2.93426 m
Height of flip bucket	4.6561 m	4.41366 m

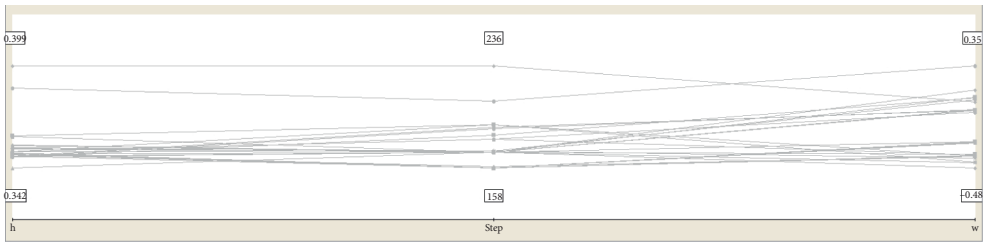

Figure 11: Relationship between numerical values and the positions (h) w, and step.

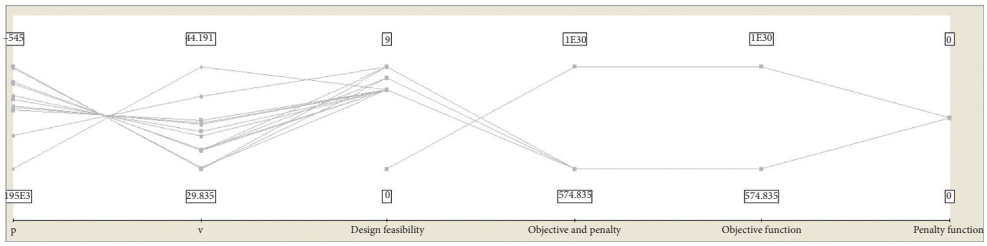

Figure 12: Relationship between the numerical values (p) w, design feasibility, objective and penalty, objective function, and penalty.

between the pressures at falling points and the sizes of different flip buckets, aiming to identify the size that has the greatest influence on the pressure at the falling point. Similarly, attention should be paid to the relationship between the flow velocities of the falling points and the sizes of different flip buckets, identifying the size that has the most influence on the kinetic energy of the falling point. By doing this, the determined model size can be used in the optimization, providing an important reference for any modification of the model design. Moreover, the model size can again be used as the optimal design variable for secondary optimization, again providing important references for the selection of design variables. Multiple design variables can be subjectively selected for optimization. After the optimization, the size of some flip buckets are hardly able to influence the objective function [29–32].

4.2.3. Information Obtained from the Results Diagram. The above results diagram mainly indicates the relations among all the variables in the optimization. Variables include the overflow width, height of the flip bucket, computation time step, pressure at the falling point, velocity at the falling point, and objective functional value. The overflow width influences the scouring range of the falling points of the ski-jump flow. According to model parameterization, the height of the flip bucket is closely related to the arc angle in different models. Variations of heights directly influence the size of the arc opening. The height of the flip bucket is positively related to the degree of the opening, and the degree of the opening is positively related to the length of the flip bucket. In view of the above, the degree of the arc opening along the horizontal direction of the flip bucket is large. This indicates that the height of the flip bucket is related to different arc angles. Representing the height of the flip bucket as different arc sizes directly in an optimization can reduce the workload involved in model processing. The calculation time step mainly serves to assist in optimization, its main function being the division of time periods. Time will also influence the pressure and the velocity at falling points. Using a single time point makes it difficult to prove that the results are optimal; therefore, one time period was chosen. The pressure and the velocity at the falling points in one time period are variable, which can allow for a better interpretation of the influences of the water flow on the surface scouring. The pressure at the falling points mainly reflects the vertical scouring effects of the flow and can also influence the depth of the scouring pit. The velocity at the falling points mainly reflects the kinetic energy when the flow hits the ground surface, and it also influences the shape of the scouring pit. The objective functional value mainly reflects the comprehensive value of the two objectives. Finally, the above result diagram was analyzed. Numerical relation diagrams of different variables were drawn (Figures 11 and 12). The two-dimensional and three-dimensional contour maps of the relations of the overflow width and height of the flip bucket with pressure and flow velocity at the falling points are shown in Figures 13–15, and

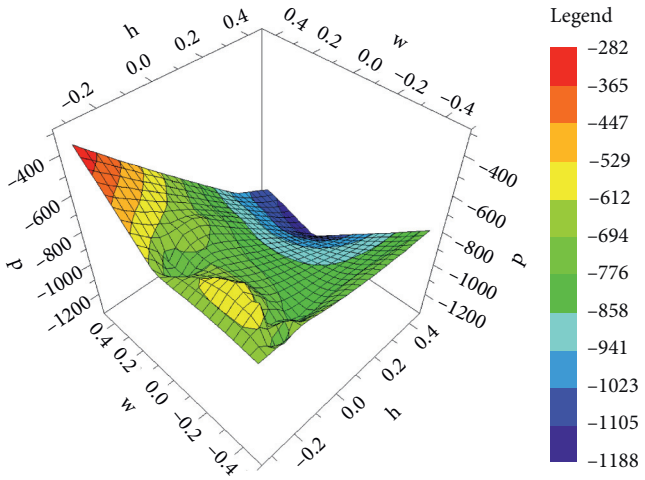

Figure 13: Contour map of the three-dimensional relationship of the overflow width and height of the flip bucket with the intensity of the water pressure.

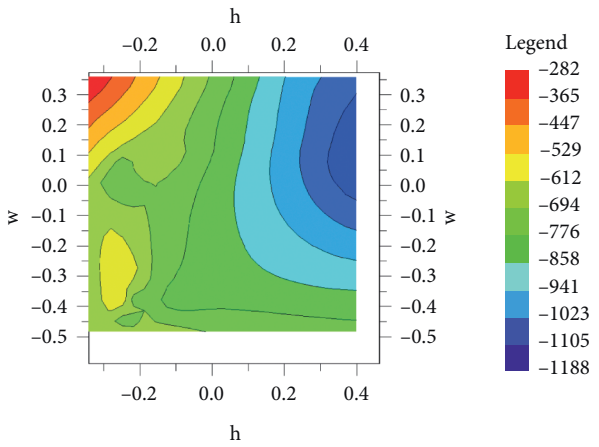

Figure 14: Contour map of the two-dimensional relationship of the overflow width and the height of the flip bucket with the intensity of the water pressure.

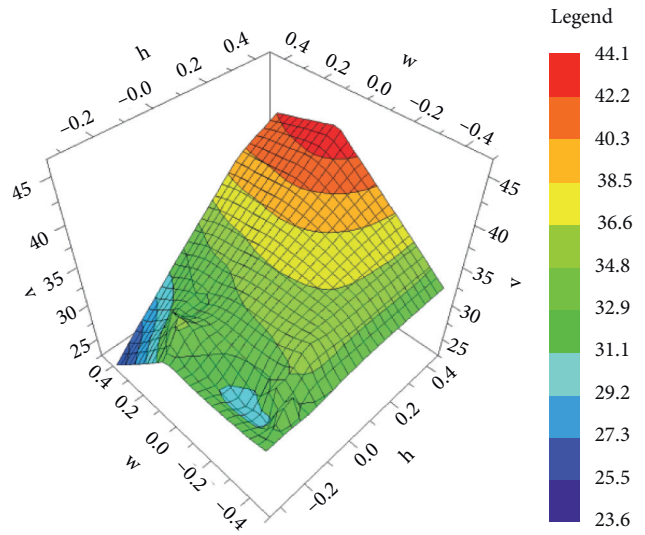

Figure 15: Contour map of the three-dimensional relationship of the overflow width and the height of the flip bucket with the flow velocity.

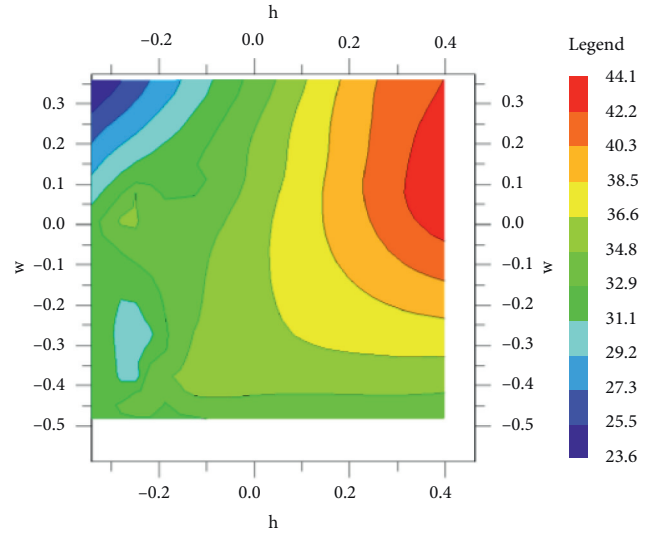

Figure 16: Contour map of the two-dimensional relationship of the overflow width and the height of the flip bucket with the flow velocity.

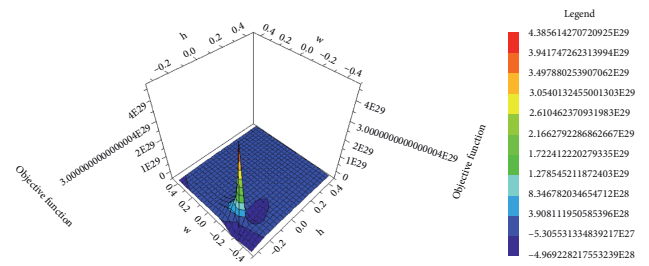

Figure 17: Contour map of the three-dimensional relationship of the overflow width and the height of the flip bucket with the objective functional value.

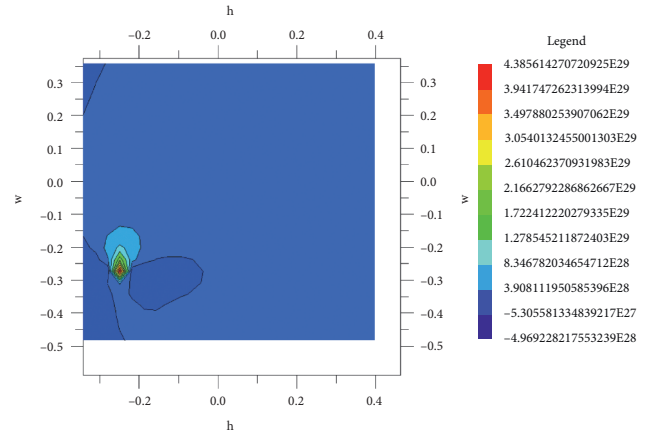

Figure 18: Contour map of the two-dimensional relationship of the overflow width and the height of the flip bucket with the objective functional value.

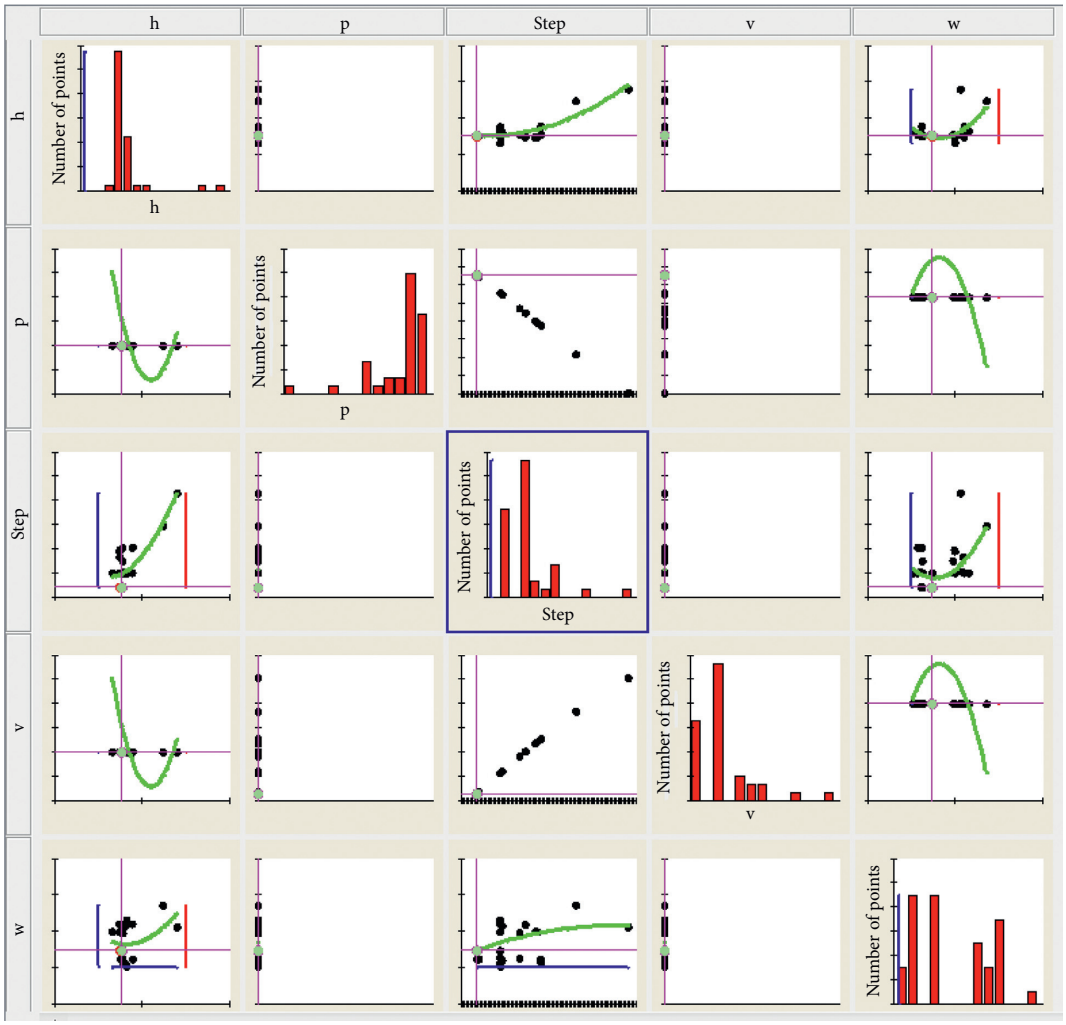

Figure 19: Two-dimensional numerical relationship matrix among different calculation parameters.

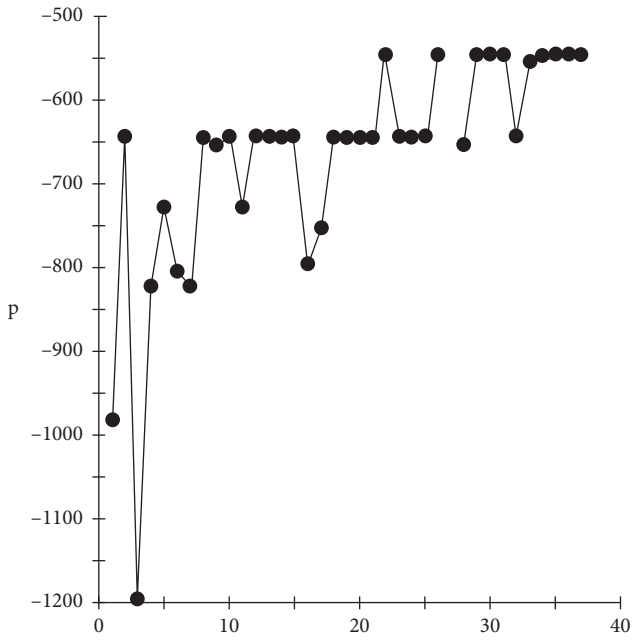

Figure 20: Optimization process of the pressure values.

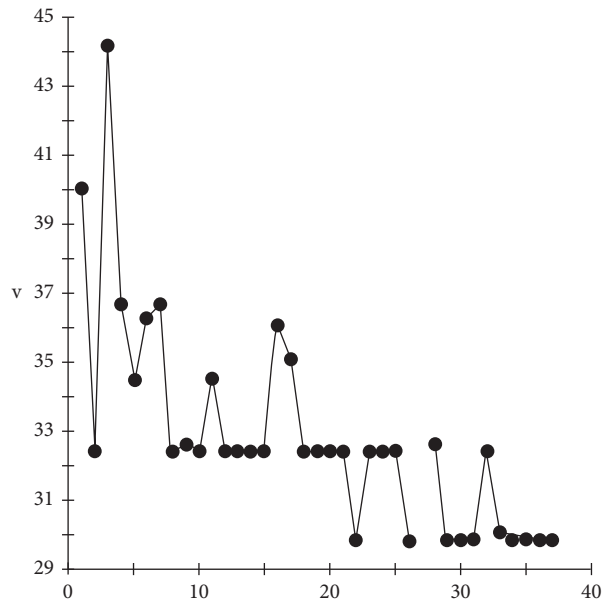

Figure 21: Optimization process of velocity.

16. Based on these maps, the influence of the shape of the flip bucket on the two optimization goals was analyzed. The two-dimensional and three-dimensional contour maps of the relations of the overflow width and the height of the flip bucket with an objective functional value (Figures 17 and 18) were used to analyze the comprehensive influence of the shape of the flip bucket on multiple objectives. The two-dimensional numerical relationship matrix among different calculation parameters (Figure 19) can identify the relations among different parameters. Finally, the optimization process of the two optimization goals (Figures 20 and 21) reveals multiple optimal solutions [33–38].

5. Conclusions

Optimization should be based on an original design scheme. The model size has to be corrected, and the relationship among different model sizes must be reflected in the mathematical relation of the model size in the original design scheme. In the design scheme, changing one model size might influence the size at other positions. Therefore, the chosen optimization variables should be representative and be able to evaluate the whole model size. Optimization seeks to improve the original design scheme. The original design schemes mainly come from experience; faced with varied real-life conditions, optimization only becomes meaningful when certain theoretical bases are combined.

In this study, a shape modification program of the flip bucket is proposed, and the results are calculated using a genetic algorithm. The results demonstrated that the optimal design scheme produces a weaker scouring force from water flowing onto the ground compared with the original scheme, indicating the reasonability of the optimization results.

The path and location of the high-speed water flow significantly influence the environment. Regarding the size of the flip bucket, it can be concluded that the water flow direction can be changed by changing the model size of the flip bucket or by splitting one flow into two so as to prevent landslides due to a scouring effect, thereby protecting the environment and the ecosystem from damage [19, 39–42].

Data Availability

All data generated or analyzed during this study are included in this published article.

Conflicts of Interest

The authors declare no conflicts of interest.

Acknowledgments

This study was funded by the National Natural Science Foundation of China (grant no. 51579089).

References

[1] S. Qian, "Ski-jump-step energy dissipators," in *Proceedings of The 35th Iahr World Congress*, pp. 471–480, Chengdu, China, September 2013.

[2] G. Huang, S. Xie, and W. Duan, "Optimization and application of energy dissipation works for ski jump spillway at high dams," *Journal of Yangtze River Scientific Research Institute*, vol. 28, no. 10, pp. 90–93, 2011.

[3] X. Zhang, C. Liang, Q. Fu, and X. Zhang, "Application of energy approach to estimating scour depth," *Journal of Sichuan University.Engineering Science Edition*, vol. 35, no. 2, pp. 27–30, 2003.

[4] Z. Liu, H. Liu, S. Sun et al., "Study on flood discharge atomization of ski-jump energy dissipation scheme for reconstruction project of Fengman Hydropower Station," *Water Resources and Hydropower Engineering*, vol. 49, no. 1, pp. 108–113, 2018.

[5] J.-h. Wu, S.-t. Qian, and F. Ma, "A new design of ski-jump-step spillway," *Journal of Hydrodynamics*, vol. 28, no. 5, pp. 914–917, 2016.

[6] J. Deng, Z. Yang, Z. Tian et al., "A new type of leak-floor flip bucket," *Science China Technological Sciences*, vol. 59, no. 4, pp. 565–572, 2016.

[7] A. Parsaie, S. Dehdar-Behbahani, and A. H. Haghiabi, "Numerical modeling of cavitation on spillway's flip bucket," *Frontiers of Structural And Civil Engineering*, vol. 10, no. 4, pp. 438–444, 2016.

[8] A. Parsaie, A. H. Haghiabi, and A. Moradinejad, "CFD modeling of flow pattern in spillway's approach channel," *Sustainable Water Resources Management*, vol. 1, no. 3, pp. 245–251, 2015.

[9] A. Parsaie, A. Moradinejad, and A. H. Haghiabi, "Numerical modeling of flow pattern in spillway approach channel," *Jordan Journal of Civil Engineering*, vol. 12, no. 1, pp. 1–9, 2018.

[10] A. Parsaie, S. Ememgholizadeh, A. H. Haghiabi, and A. Moradinejad, "Investigation of trap efficiency of retention dams," *Water Supply*, vol. 18, no. 2, pp. 450–459, 2018.

[11] A. Parsaie and A. H. Haghiabi, "Numerical routing of tracer concentrations in rivers with stagnant zones," *Water Supply*, vol. 17, no. 3, pp. 825–834, 2017.

[12] A. Parsaie, H. M. Azamathulla, and A. H. Haghiabi, "Physical and numerical modeling of performance of detention dams," *Journal of Hydrology*, vol. 581, p. 121757, 2020.

[13] S. Dehdar-behbahani and A. Parsaie, "Numerical modeling of flow pattern in dam spillway's guide wall. Case study: balaroud dam, Iran," *Alexandria Engineering Journal*, vol. 55, no. 1, pp. 467–473, 2016.

[14] A. Zhu, T. Huang, Y. Zhang, and L. Lang, "Study on ski-jump energy dissipation scheme for lower reservoir of Zhouning Pumped Storage Hydropower Station," *Water Resources and Hydropower Engineering*, vol. 47, no. 10, pp. 34–39, 2016.

[15] W. Gou, H. Li, Y. Du et al., "Effect of sediment concentration on hydraulic characteristics of energy dissipation in a falling turbulent jet," *Applied Sciences-Basel*, vol. 8, p. 9, 2018.

[16] R. d. Lara, J. J. Ota, and A. L. T. Fabiani, "Reduction of the erosive effects of effluent jets from spillways by contractions in the flow," *Rbrh*, vol. 23, p. 11, 2018.

[17] J. Deng, W. Wei, Z. Tian, and F. Zhang, "Design of A Streamwise-Lateral ski-jump flow discharge spillway," *WATER*, vol. 10, p. 11, 2018.

[18] W. Cheng, Q. Yang, and Z. Chang, "Application of leak-floor flip bucket to spillway for Lijiayan Reservoir," *Water Resources and Hydropower Engineering*, vol. 49, no. 4, pp. 63–69, 2018.

[19] J. Lian, X. Wang, W. Zhang, B. Ma, and D. Liu, "Multi-source generation mechanisms for low frequency noise induced by flood discharge and energy dissipation from a high dam with a ski-jump type spillway," *International Journal of Environmental Research And Public Health*, vol. 14, p. 12, 2017.

[20] C. Han, J. Zhao, Y. Dang, and F. Sun, "Hydraulic control OF safe operation OF large-scaled hypervelocity discharge tunnel," *Advances In Water Resources And Hydraulic Engineering*, vol. 1-6, pp. 1556–1561, 2009.

[21] J.-h. Wu, X.-y. Zhang, F. Ma, and W.-w. Wu, "Ski jump trajectory with consideration of air resistance," *Journal of Hydrodynamics*, vol. 27, no. 3, pp. 465–468, 2015.

[22] S. Qian, J. Wu, and F. Ma, "Hydraulic performance of ski-jump-step energy dissipater," *Journal Of Hydraulic Engineering*, vol. 142, p. 10, 2016.

[23] P. ZOU, J. WANG, and H. YIN, "Research on dynamic characteristics of original rock in the scour pit of energy dissipation of ski-jump," *Journal of Hydroelectric Engineering*, vol. 26, no. 4, pp. 71–75, 2007.

[24] Z. Chen, Y. Chen, and G. Huang, "Research of configuration of narrow opening skijump spillway and estimation of logitudinally extended width of jet," *Journal of Yangtze River Scientific Research Institute*, vol. 19, no. 4, pp. 11–14, 2002.

[25] J. Feng, L. Wang, R. Li, K. Li, X. Pu, and Y. Li, "Operational regulation of a hydropower cascade based on the mitigation of the total dissolved gas supersaturation," *Ecological Indicators*, vol. 92, pp. 124–132, 2018.

[26] Z. Li, C. Bai, and W. Zhang, "Optimum test on bucket dissipation of bashan hydropower station's overflow spillway," *Journal of Yunnan Agricultural University*, vol. 25, no. 5, pp. 706–711, 2010.

[27] S. H. Hojjati, S. A. A. Salehi Neyshabouri, and S. A. A. S. Neyshabouri, "The objective design of triangular bucket for dam's spillway using Non-dominated Sorting Genetic Algorithm II: nsga-II," *Scientia Iranica*, vol. 24, no. 1, pp. 19–27, 2017.

[28] Y. Wang, C. Jiang, R. Liao, and Y. Yang, "Effect of different outlet shapes of spillway tunnel on ski-jump energy dissipation," *Journal of Hydroelectric Engineering*, vol. 34, no. 8, pp. 70–76, 2015.

[29] A. H. Haghiabi, "Estimation of scour downstream of a ski-jump bucket using the multivariate adaptive regression splines," *Scientia Iranica*, vol. 24, no. 4, pp. 1789–1801, 2017.

[30] F. T. Buffon and M. G. Marques, "Método de determinação de pressões em bacias de dissipação a jusante de vertedores tipo salto esqui," *Rbrh*, vol. 21, no. 3, pp. 576–586, 2016.

[31] W.-r. Wei, J. Deng, and B. Liu, "Influence of aeration and initial water thickness on axial velocity attenuation of jet flows," *Journal of Zhejiang University Science A*, vol. 14, no. 5, pp. 362–370, 2013.

[32] J. Lucas, W. H. Hager, and R. M. Boes, "Deflector effect on chute flow," *Journal of Hydraulic Engineering*, vol. 139, no. 4, pp. 444–449, 2013.

[33] V. C. Putton, C. Marson, V. Fiorotto, and E. Caroni, "Supercritical flow over a dentated sill," *Journal Of Hydraulic Engineering-ASCE*, vol. 137, no. 9, pp. 1019–1026, 2011.

[34] M. Ribeiro, J. Boillat, A. Schleiss, and F. Laugier, "Coupled spillway devices and energy dissipation system at St-Marc Dam (France)," *Labyrinth and Piano Key Weirs*, vol. 1, pp. 113–121, 2011.

[35] Q. Yuan, X. Wang, and S. Luo, "The application of two-phase flow numerical simulation in fengman dam overall treatment project," *Advances In Hydraulic Physical Modeling And Field Investment And Investigation*, vol. 1, pp. 217–221, 2010.

[36] R. Steiner, V. Heller, W. H. Hager, H.-E. Minor, and H. Minor, "Deflector ski jump hydraulics," *Journal of Hydraulic Engineering*, vol. 134, no. 5, pp. 562–571, 2008.

[37] R. Pardo-Gomez, "Proposed method for the hydraulic design of ski-jump energy dissipators in dam spillways, considering the occurrence of scour holes downstream of the structure," *Ingenieria Hidraulica En Mexico*, vol. 23, no. 2, pp. 111–121, 2008.

[38] L. Schmocker, M. Pfister, W. H. Hager, and H.-E. Minor, "Aeration characteristics of ski jump jets," *Journal of Hydraulic Engineering*, vol. 134, no. 1, pp. 90–97, 2008.

[39] L. Zhou, W. Guo, B. Yan, Y. Dong, and H. Li, "The ski-jump energy dissipation of scour hole test on curving spillway," *Journal of Shenyang Agricultural University*, vol. 39, no. 3, pp. 336–339, 2008.

[40] W. Huai, Y. Zeng, H. Li, and L. Huang, "Experimental research on crest spillway flood energy dissipation for the double-curvature arch dam," *Journal of Sichuan University. Engineering Science Edition*, vol. 39, no. 1, pp. 1–5, 2007.

[41] V. Heller, W. H. Hager, and H.-E. Minor, "Ski jump hydraulics," *Journal of Hydraulic Engineering*, vol. 131, no. 5, pp. 347–355, 2005.

[42] H. Yu and Z. Sun, "The pattern selection for the first extraordinary spillway of removing danger and reinforce engineering of dahuofang reservoir," *Journal of Shenyang Agricultural University*, vol. 35, no. 5/6, pp. 549–551, 2004.